Partial Aircraft State Estimation from Optical Flow Using Non-Model-Based Optimization

Joseph J. Kehoe, Ryan S. Causey, Amanda Arvai and Rick Lind
University of Florida

***Abstract*— Computer vision is an enabling technology for autonomous micro aerial vehicle (MAV) applications. This paper presents an approach for the estimation of aircraft angular rates and wind-axis angles using monocular vision. The solution is obtained through nonlinear optimization techniques applied to the optical flow of tracked feature points in the image. The coupled equations of motion for an aircraft and image-based features are developed and utilized to establish a mathematical framework for the estimation process. The technique is then demonstrated in simulation.**

I. INTRODUCTION

Unmanned aerial vehicles (UAVs) have been considered for a variety of applications. Recent progress in the development of small-scale, fixed wing UAVs has facilitated mission scenarios that were previously not possible. A micro aerial vehicle (MAV) exhibits the stealth and agility to maneuver undetected throughout complex and cluttered environments. Autonomous navigation of such trajectories would present an attractive capability for many envisioned tasks.

Agile autonomous flight amongst cluttered and unforeseen obstacles represents a challenging control task. While a variety of miniature inertial-measurement packages have been emerging for use in MAV applications, these units add weight and often provide inaccurate information during aggressive maneuvers. Alternatively, small video cameras present a lightweight, low-power, and information-rich sensor. Computer vision has been demonstrated as an enabling technology for MAV control tasks.

Vision processing techniques allow the extraction of information concerning both the environment as well as camera motion. In particular, techniques that can identify and track points of significance in successive images enable a variety of problems to be addressed. These "feature points" are commonly detected using the intensity gradient of the image, and are then tracked using techniques such as template registration, point correlation, dynamic filtering, or some combination thereof [1], [2], [3]. Recent efforts have moved these tracking algorithms towards real-time implementation for images with large motion between frames for flight control applications [2].

Tracking features between consecutive frames gives an indication of the perceived motion in the image. This apparent velocity is denoted optical flow and can be characterized by the gradient of the image intensity function [4]. A variety of techniques exist for computing optical flow, including differential methods, frequency-based methods, and correlation-based methods [5]. For the case of a fixed environment, optical flow results solely from camera motion and can therefore provide information related to the vehicle state.

Researchers have exploited this observation previously for state estimation. Soatto et al. derived a form of the Kalman filter that uses the relationship between vision-based measurements and the motion of the camera [6], [7]. The resulting implicit extended Kalman filter (IEKF) can be used to recover the camera motion states. Gurfil and Rotstein recast Soatto's work in terms of an aircraft state-estimation problem by incorporating aircraft dynamics into the IEKF framework [8]. The resulting formulation partially estimated the aircraft states but exhibited relatively slow convergence. Improvements have been demonstrated by Webb et al. who also used an aircraft model [9], [10]. Unfortunately, accurate MAV models are often not available within an aggressive flight regime where the aerodynamics are notoriously difficult to characterize.

The work presented here forgoes the use of a model-based approach in exchange for numerical optimization techniques. Essentially, the geometric relationship between camera motion and optical flow is utilized to solve for certain motion parameters. A similar approach was adopted in [11] where assumed knowledge of the translational motion was used to linearize the optical flow expressions. The angular rates were then determined using linear least-squares optimization.

This paper assumes no knowledge of the aircraft state. Nonlinear optimization applied to the optical flow relationships yields accurate values of the aircraft angular rates. These estimates are then used to decouple the optical flow for extraction of translational velocity components. No vehicle model is required and rapidly converging estimates can be obtained for even aggressive motions provided that enough feature points appear within the camera field of view.

The remainder of the paper is organized as follows. Section II develops the coupled equations of motion describing the dynamics of the aircraft-camera system, thus forming a mathematical basis for the remainder of the paper. Section III details the vision-based approach to state estimation using a nonlinear least-squares optimization technique. Finally, Section IV discusses a demonstrative example performed in simulation using a nonlinear aircraft model.

This work was supported by AFOSR and AFRL/MN

J. Kehoe, R. Causey, and A. Arvai are Graduate Students in the Department of Mechanical and Aerospace Engineering

R. Lind is an Assistant Professor in the Department of Mechanical and Aerospace Engineering

II. AIRCRAFT-CAMERA EQUATIONS OF MOTION

Vision-based control techniques primarily draw their signals from the focal plane. It is therefore necessary to relate the aircraft flight dynamics to focal plane dynamics within a unified framework. This framework will provide a general starting point for the mathematical formulation and solution of a variety of vision-based flight control problems [12].

A. Problem Geometry

The geometry for the general case of an aircraft carrying a single camera is described by the vector diagram of Fig. 1 and (1a)-(1d). The aircraft body basis, **B**, is fixed at the aircraft center of gravity and is located relative to the inertial frame, **E**, by the vector $\vec{R}$ as in (1a). The camera reference frame, **C**, is fixed to the aircraft at an arbitrary position and is located relative to **B** by the vector $\vec{\Delta}$ as in (1b).

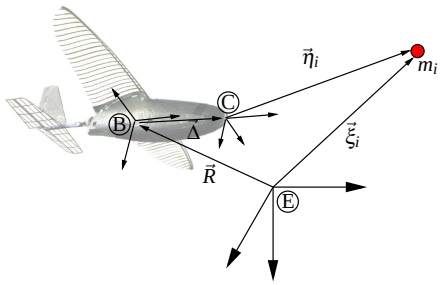

Fig. 1. Geometry Exhibited by Aircraft, Camera, and a Feature Point

$$\vec{R} = R_1\hat{e}_1 + R_2\hat{e}_2 + R_3\hat{e}_3 \tag{1a}$$

$$\vec{\Delta} = \Delta_1\hat{b}_1 + \Delta_2\hat{b}_2 + \Delta_3\hat{b}_3 \tag{1b}$$

$$\vec{\xi}_i = \xi_{1_i}\hat{e}_1 + \xi_{2_i}\hat{e}_2 + \xi_{3_i}\hat{e}_3 \tag{1c}$$

$$\vec{\eta}_i = \eta_{1_i}\hat{c}_1 + \eta_{2_i}\hat{c}_2 + \eta_{3_i}\hat{c}_3 \tag{1d}$$

The i^{th} point-feature of the environment is denoted m_i and is located relative to **E** by $\vec{\xi}_i$ as in (1c). The vector $\vec{\eta}_i$ then relates the relative position of m_i with respect to **C**, as described by (1d). This relative position vector can be expressed in terms of the aircraft position and orientation via the coordinate transformations T_{EB} and T_{BC}, which represent simple axis rotations from **E** to **B** and **B** to **C**, respectively. Using (2), $\vec{R}$, $\vec{\Delta}$, and $\vec{\xi}$ are all transformed to the **C** basis, thus introducing the aircraft position and orientation into the expression for $\vec{\eta}$.

$$\vec{\eta}_i = T_{BC}T_{EB}(\vec{\xi}_i - \vec{R}) - T_{BC}\vec{\Delta} \tag{2}$$

B. Focal Plane Dynamics

The perspective camera model maps the projection of m_i to the focal plane through a transformation that is dependent upon both the relative position, $\vec{\eta}$, and the focal length, f. The focal length is a constant intrinsic camera parameter that measures the distance from the origin of **C** to the focal plane along the $\hat{c}_3$ axis. This axis is normal to the focal plane. The geometry of this mapping is depicted in Fig. 2. The projection of m_i is located on the focal plane by the coordinates μ_i and ν_i which are determined as in (3). The actual mapping to an image is restricted by the field of view such that $\mu \in [\underline{\mu}, \overline{\mu}]$ and $\nu \in [\underline{\nu}, \overline{\nu}]$.

$$\begin{bmatrix} \mu_i \\ \nu_i \end{bmatrix} = \frac{f}{\eta_{3_i}} \begin{bmatrix} \eta_{1_i} \\ \eta_{2_i} \end{bmatrix} \tag{3}$$

Inspection of Fig. 2 and the expression in (3) reveals that μ_i and ν_i are proportional to the tangent of the bearing and elevation to m_i. Consequently, depth information is lost and the image can be used only to locate the line of sight to m_i for a given image frame.

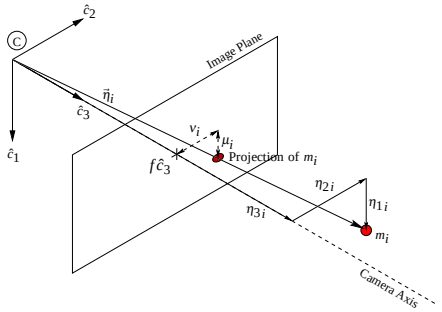

Fig. 2. Mapping m_i to the Focal Plane

The velocity of m_i's projection in the image is found through differentiation of (3). Here, the focal plane velocities are interpreted as the optical flow of the image sampled at the point (μ_i, ν_i). This quantity can be measured directly from video data for a set of n points given that each point can be tracked between two image frames. A variety of techniques discussed in the vision processing literature have been shown to successfully detect and track feature points through a series of images [1], [2], [3].

$$\begin{bmatrix} \dot{\mu}_i \\ \dot{\nu}_i \end{bmatrix} = \frac{f}{{\eta_{3_i}}^2} \begin{bmatrix} \eta_{3_i} & 0 & -\eta_{1_i} \\ 0 & \eta_{3_i} & -\eta_{2_i} \end{bmatrix} \begin{bmatrix} \dot{\eta}_{1_i} \\ \dot{\eta}_{2_i} \\ \dot{\eta}_{3_i} \end{bmatrix} \tag{4}$$

C. The Coupled Equations

It is evident through inspection of (3) and (4) that $(\dot{\mu}_i, \dot{\nu}_i)$ can be described in terms of aircraft parameters through the transformations T_{EB} and T_{BC} if $\vec{\eta}_i$ is expressed as in (2). Equation (4) indicates the necessity to differentiate $\vec{\eta}_i$. The derivative is taken prior to the coordinate transformation with respect to the **E** reference frame. The assumption is made that m_i is static in the **E**-frame for each of the i feature points. The camera is also assumed to have a fixed position relative to **B**. These assumptions imply that $\frac{^E d}{dt}(\vec{\xi}) = \frac{^B d}{dt}(\vec{\Delta}) = 0$ in (5). Evaluation of the remaining terms yields the time derivative of $\vec{\eta}_i$ with respect to the **C** frame as shown in (6) where $^E\vec{\omega}^B$ and $^B\vec{\omega}^C$ represent the angular velocities of the **B**-frame and **C**-frame with respect to **E** and **B**, respectively. These angular velocities are expressed in their respective rotating bases.

$$\frac{^E d}{dt}(\vec{\eta}) = \frac{^E d}{dt}\left(\vec{\xi}\right) - \frac{^E d}{dt}\left(\vec{R}\right) - \frac{^E d}{dt}\left(\vec{\Delta}\right) \tag{5}$$

$$\frac{^C d}{dt}(\vec{\eta}) = -\left(\dot{\vec{R}} + {}^E\vec{\omega}^B \times \vec{\Delta}\right) - \left({}^E\vec{\omega}^B + {}^B\vec{\omega}^C\right) \times \vec{\eta} \tag{6}$$

The resulting differential equation describes the relative position and orientation changes between **C** and the m_i. This result is expressed in terms of aircraft states following the series of coordinate transformations shown in (7). The dynamics of feature motion across the focal plane can now be combined with the aircraft dynamics to form a fully-coupled system. Coupling is accomplished through augmenting the well-known aircraft equations of motion with (7) in state-space representation.

$$\dot{\vec{\eta}} = -T_{BC}\left(T_{EB}\dot{\vec{R}} + {}^{E}\vec{\omega}^{B} \times \vec{\Delta}\right) - \left(T_{BC}\,{}^{E}\vec{\omega}^{B} + {}^{B}\vec{\omega}^{C}\right) \times \vec{\eta} \qquad (7)$$

Alternatively, the feature point dynamics can be rewritten in terms of (μ_i, ν_i) using (4). Substitution yields a set of two differential equations that could augment the aircraft system as an equivalent form of (7). This form is more useful in the sense that the coupled dynamics are now represented in terms of the measurable focal-plane coordinates.

III. STATE ESTIMATION

The general expression for the focal plane velocities of a feature point is given by (4). The developments of Section II-C allow this general expression to be rewritten in terms of aircraft states. First, the assumption is made that the camera has fixed position and orientation at the origin of **B** and hence $\vec{\Delta} = \dot{\vec{\Delta}} = {}^{B}\vec{\omega}^{C} = \vec{0}$.

In addition, T_{BC} is chosen such that the camera axis, $\hat{c}_3$, coincides with the body x-axis, $\hat{b}_1$. This configuration has the camera pointed directly out the nose of the aircraft. The transformation is given by (8).

$$T_{BC} = \begin{bmatrix} 0 & 0 & 1 \\ 0 & -1 & 0 \\ 1 & 0 & 0 \end{bmatrix} \qquad (8)$$

These simplifying assumptions do not affect the generality of the following analysis but facilitate clarity. After substitution of (2), (3) and (7) into (4), the focal plane velocities take on the form shown by (9) for an aircraft [12]. This form relates $(\dot{\mu}_i, \dot{\nu}_i)$ in terms of (μ_i, ν_i), the aircraft body-axis velocities and rates, (u, v, w, p, q, r), and the range to m_i, η_{3_i}.

$$\begin{bmatrix} \dot{\mu}_i \\ \dot{\nu}_i \end{bmatrix} = f \begin{bmatrix} \frac{\mu_i}{\eta_{3i}} & 0 & \frac{-1}{\eta_{3i}} & \nu_i & (1+\mu_i{}^2) & \mu_i\nu_i \\ \frac{\nu_i}{\eta_{3i}} & \frac{1}{\eta_{3i}} & 0 & -\mu_i & \mu_i\nu_i & (1+\nu_i{}^2) \end{bmatrix} \begin{bmatrix} u \\ v \\ w \\ p \\ q \\ r \end{bmatrix} \qquad (9)$$

The assumption is also made that the camera is calibrated. Therefore the focal length, f, is a known parameter and can be normalized to $f = 1$.

Given the measured focal-plane position and velocity of m_i's projection, the remaining unknown terms in (9) consist of the three aircraft translational velocity components $\{u,\ v,\ w\}$, the three aircraft angular velocity components $\{p,\ q,\ r\}$, and the range component $\{\eta_{3_i}\}$ of the feature's relative position vector. Thus there are only two equations in six unknowns; however, tracking an additional feature point, $m_{(i+1)}$, introduces only a single additional unknown, $\eta_{3(i+1)}$, while providing two additional equations. The translational velocities and angular rates are common to the new expressions because the $m_{(i+1)}$ is tracked relative to the same reference frame as m_i. Therefore, tracking n features gives $2n$ equations in $6+n$ unknowns. Consequently, the system is completely determined for $n \geq 6$.

A. Angular Rates

The observed relationship between aircraft states and measured focal plane data is exploited using a nonlinear least-squares routine. A cost function is formulated using a vector-valued function, $\vec{J}(\vec{x})$, which relates each of the n measured focal-plane velocities to the theoretical values determined by the unknown aircraft states and feature ranges through (9). This function is expressed as in (10).

$$\vec{J}(\vec{x}) = \begin{bmatrix} \dot{\mu}_1 - \left(\frac{\mu_1}{x_7}x_1 - \frac{1}{x_7}x_3 + \nu_1 x_4 + (1+\mu_1{}^2)x_5 + \mu_1\nu_1 x_6\right) \\ \dot{\nu}_1 - \left(\frac{\nu_1}{x_7}x_1 + \frac{1}{x_7}x_2 - \mu_1 x_4 + \mu_1\nu_1 x_5 + (1+\nu_1{}^2)x_6\right) \\ \vdots \\ \dot{\mu}_n - \left(\frac{\mu_n}{x_{(6+n)}}x_1 - \frac{1}{x_{(6+n)}}x_3 + \nu_n x_4 + (1+\mu_n{}^2)x_5 + \mu_n\nu_n x_6\right) \\ \dot{\nu}_n - \left(\frac{\nu_n}{x_{(6+n)}}x_1 + \frac{1}{x_{(6+n)}}x_2 - \mu_n x_4 + \mu_n\nu_n x_5 + (1+\nu_n{}^2)x_6\right) \end{bmatrix} \qquad (10)$$

where

$$\vec{x} = \begin{bmatrix} u & v & w & p & q & r & \eta_{3_1} & \cdots & \eta_{3_n} \end{bmatrix}^T$$

The estimated vector, $\hat{\vec{x}}$, is found through solving the optimization problem posed in (11) that minimizes the magnitude of the cost function.

$$\hat{\vec{x}} = \arg \min_{x \in \mathbb{R}^{(6+n)}} \frac{1}{2} \parallel \vec{J}(\vec{x}) \parallel^2 \qquad (11)$$

The focal-plane velocities are linear in the aircraft translational and angular velocities for the case of known 3-D feature-point locations as shown by (9). When these 3-D locations are not available, as considered here, a nonlinearity is introduced into the expressions through the unknown range to each feature point, η_{3_i}. This nonlinearity appears in (9) as an inverse relationship that scales the terms associated with aircraft translational velocity. Essentially, the value of η_{3_i} associated with m_i determines the contribution of the aircraft translational velocities to the total optical flow at (μ_i, ν_i). Inspection of (9) verifies that feature points corresponding to distant m_i will exhibit optical flow dominated by aircraft orientation changes while nearby m_i will be dominated by aircraft translational motion.

The composition of the optical flow at (μ_i, ν_i) resulting from translational and angular velocity components affects the accuracy of the optimization in (11). This issue deals with the well-known requirement for sufficient parallax in vision-based estimation problems [13]. Parallax refers to perceived motion resulting from a change in observer position. The optical flow due to each of the translational velocities induces greater parallax when m_i corresponds to a feature at close range; however, previous discussion indicates that the optical

flow induced by angular motion might be poorly scaled in this case. This observation suggests that the accuracy of the state estimates could be improved through selective inclusion of feature points in the optimization. A tradeoff is present in that nearby points exhibiting large parallax must be balanced with distant points that allow adequate representation of the angular motion of the vehicle.

Defining a selection strategy to meet these criteria is problematic due to the unknown range value to each point, η_{3_i}; however, the relationships exhibited in (9) coupled with generalized behavior can yield a policy to select features that are likely to achieve the desired balance. For example, (9) shows that the translational velocities have a greater contribution to the optical flow at large radial distance from the image center. Further, u causes points to spread radially from the direction of velocity. The velocities v and w cause horizontal and vertical motion, respectively, for the given choice of T_{BC}. The roll rate, p, induces a "swirling" motion about the axis of rotation that increases in magnitude with radial distance from this axis. Finally, q and r cause vertical and horizontal motion, respectively.

Based on these observations, areas of the image are defined from which feature-point selection is desired. Points are restricted radially in the image to an annulus such that sufficient parallax is exhibited without choosing points that are likely to dominate the optical flow. Further, points are selected within this annulus from angular regions centered about the equidistant lines from the horizontal and vertical axes (i.e. along the diagonals). This restriction avoids the ambiguity resulting from similar focal-plane motions induced by $\{v,w\}$ and {q,r}. These regions are depicted in Fig. 3.

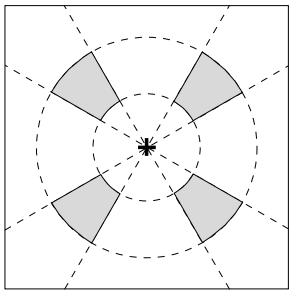

Fig. 3. Image Regions for Feature-Point Selection (shaded)

Despite these efforts to condition the optimization, estimation of the translational velocities remains problematic. The inverse scaling on η_{3_i} for these states in (9) implies a nonunique solution for the set of unknowns, $\{u,\ v,\ w,\ \eta_{3_i}\}$. Therefore the total translational velocity can only be determined up to a scaling constant using this procedure. This phenomenon is well documented in the literature [6], [7], [8], [13]. Moreover, another difficulty arises in that the scale difference between u and $\{v,w\}$ is typically large for fixed-wing aircraft. So while the optimization procedure is capable of determining accurate estimates for the aircraft angular velocities, further analysis is required to obtain reasonable velocity estimates.

B. Aerodynamic Angles

Although the nonlinear estimation of Section III-A yielded only a subset of the desired estimates, the information that was obtained can be used to extract further details from the raw image sequence. Specifically, the focal-plane velocities described by (9) can be decomposed into two components: one resulting from aircraft orientation changes and the other resulting from aircraft translation [14]. This additional information is then used to estimate the aircraft angle of attack, α, and angle of sideslip, β. These aerodynamic angles describe the orientation of the velocity vector with respect to the aircraft body x-axis, $\hat{b}_1$, and therefore relate the side and vertical velocity components, v and w.

Computation of the decoupled optical flow is possible for the measured focal plane positions and velocities if reasonable estimates for the angular rates are available resulting from the analysis of Section III-A. The optical flow component due to aircraft rotation is found as in (12).

$$\begin{bmatrix} \dot{\mu}_{R_i} \\ \dot{\nu}_{R_i} \end{bmatrix} = f \begin{bmatrix} \nu_i & (1+\mu_i{}^2) & \mu_i\nu_i \\ -\mu_i & \mu_i\nu_i & (1+\nu_i{}^2) \end{bmatrix} \begin{bmatrix} p \\ q \\ r \end{bmatrix} \quad (12)$$

The optical flow component due to translational motion cannot be found explicitly from (9) due to the ambiguity between the linear aircraft velocities and the range to each individual feature. The result of (12) is therefore used to determine this remaining translational component, as in (13).

$$\begin{bmatrix} \dot{\mu}_{T_i} \\ \dot{\nu}_{T_i} \end{bmatrix} = \begin{bmatrix} \dot{\mu}_i - \dot{\mu}_{R_i} \\ \dot{\nu}_i - \dot{\nu}_{R_i} \end{bmatrix} \quad (13)$$

The translational optical flow vectors will all radiate from a singular point in the image plane which is commonly denoted the focus of expansion (FOE). The FOE has zero translational optical flow and can be interpreted as the focal-plane projection of the direction of translational motion [15]. The concept is depicted in Fig. 4 where the FOE is located at focal coordinates of (μ_F, ν_F).

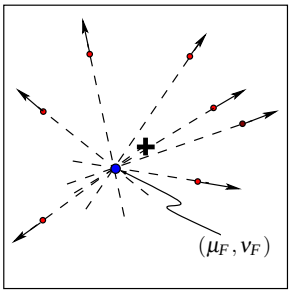

Fig. 4. Approximating the FOE using Decoupled Optical Flow

An approximation for the FOE location is found by extending the translational optical-flow vectors and seeking the common point of intersection. Using n feature points results in a system of n equations in 2 unknowns. To account for possible measurement error, a linear least-squares optimization is used as in (14).

$$\begin{bmatrix} \mu_F \\ \nu_F \end{bmatrix} = \arg \min_{\substack{\mu \in [\underline{\mu}, \overline{\mu}] \\ \nu \in [\underline{\nu}, \overline{\nu}]}} \frac{1}{2} \| C \begin{bmatrix} \mu \\ \nu \end{bmatrix} - d \|^2 \qquad (14)$$

where

$$C = \begin{bmatrix} \frac{\Delta \nu_{t_1}}{\Delta \mu_{t_1}} & \frac{\Delta \nu_{t_2}}{\Delta \mu_{t_2}} & \cdots & \frac{\Delta \nu_{t_n}}{\Delta \mu_{t_n}} \\ -1 & -1 & \cdots & -1 \end{bmatrix}^T \qquad (15a)$$

$$d = \begin{bmatrix} \left(\nu_1 - \frac{\Delta \nu_{t_1}}{\Delta \mu_{t_1}} \mu_1\right) & \left(\nu_2 - \frac{\Delta \nu_{t_2}}{\Delta \mu_{t_2}} \mu_2\right) & \cdots & \left(\nu_n - \frac{\Delta \nu_{t_n}}{\Delta \mu_{t_n}} \mu_n\right) \end{bmatrix}^T \qquad (15b)$$

Once an approximation is found for the FOE, estimates of α and β are straightforward to compute. The camera model of (3) gives directional information in the form of tangent to line of sight. Therefore, α and β are found from the coordinates of the FOE using (16a) and (16b).

$$\alpha = -\tan^{-1}\left(\frac{1}{f}\mu_F\right) \qquad (16a)$$

$$\beta = \tan^{-1}\left(\frac{1}{f}\nu_F\right) \qquad (16b)$$

While α and β are often sufficient for flight control applications, the aerodynamic relationship between these angles and $\{u,\ v,\ w\}$ can be used to form estimates of the translational velocities. This relationship is shown in (17a) - (17c), where V_T represents the total vehicle velocity.

$$\tan(\alpha) = \frac{w}{u} \qquad (17a)$$

$$\sin(\beta) = \frac{v}{V_T} \qquad (17b)$$

$$V_T = \sqrt{u^2 + v^2 + w^2} \qquad (17c)$$

The application of (17a) - (17c) leaves one variable undetermined. Therefore, approximations of v and w are computed using the assumptions described by (18). Essentially, the forward velocity component, u, is approximated as the total velocity, V_T. This approximation is reasonable for an aircraft in flight. The approximated trim velocity, $V_{T_{trim}}$, is used as the total velocity. This approximated trim velocity is chosen using known correlation to a throttle setting.

Equation (17c) is also used to help refine the estimate of u from the assumed constant value. These assumptions will affect the estimates of v and w only slightly with more significant error appearing in the estimate for u.

$$u \approx V_T \approx V_{T_{trim}} \qquad (18)$$

IV. Example

A. Simulation

Aircraft states are estimated using simulated data to demonstrate the technique. Specifically, a high-fidelity nonlinear model of an F-16 is simulated to fly through a region of obstacles [16]. A camera is mounted at the center of gravity of this aircraft, which is the origin of the **B**-basis, and aligned along the nose. The environment is constructed to provide an idealistic uniform spacing of feature points along a 3-D grid. As such, at least 24 feature points are visible and can tracked in each image frame throughout the simulation.

The flight condition is chosen as trim for straight and level flight at sea level. The airspeed is 600 *ft/sec* for which the angle of attack is 1.5625 *deg*. Doublets are commanded to elevator, aileron, and rudder control surfaces to generate maneuvers away from this trim condition.

The optimization routine solves for the 6 unknown aircraft states using the 48 equations associated with the 24 feature points. The initial conditions for these states are randomly chosen to mimic a situation in which no inertial measurements are available. Each successive estimate is then used to start the optimization at the next instant in time.

Also, the range to each feature point is estimated by the optimization procedure. The initial condition for the routine is a scaled constant. The range obviously changes as the aircraft approaches the feature point; consequently, the estimated range is not used to start the optimization for the next instant in time. The simulation actually uses this same constant as the initial condition of range for the optimization at all points in time.

B. Estimates from Optical Flow

The aircraft states are estimated through the optimization of (11). This procedure directly uses the optical flow of feature points to compute the states. The resulting estimates indicate the aircraft states throughout the maneuvers.

The estimates of body-axis translational velocities, as shown in Fig. 5, show varying levels of accuracy. The side and vertical components, v and w, exhibit the correct trend but have incorrect magnitude. The forward component, u, tracks especially poorly.

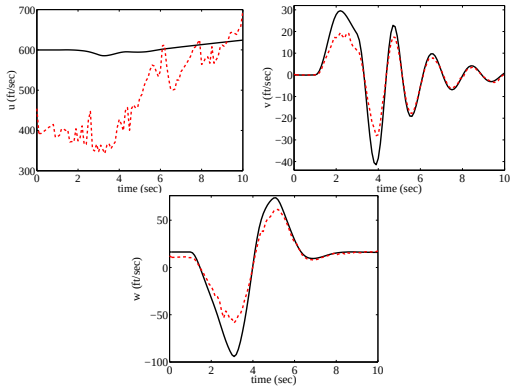

Fig. 5. Body Axis Velocities (solid) and Estimates (dashed)

The estimates of body-axis angular velocities, as shown in Fig. 6, are quite accurate. Each of those parameters is estimated to high accuracy for both large and small values during the maneuver.

C. Estimates from Decoupled Optical Flow

The states are also estimated using the decoupled optical flow which separates rotational and translational components.

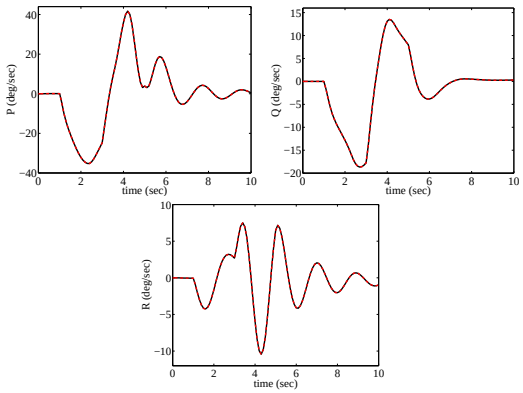

Fig. 6. Body Axis Angular Rates (solid) and Estimates (dashed)

The procedure involves extending the vectors associated with the translational optic flow and computing a common intersection point to approximate the FOE. The coordinates of this FOE, (μ_F, ν_F), are substituted into (16a) and (16b) to calculate estimates of α and β.

The resulting estimates of angle of attack and angle of sideslip, as shown in Fig. 6, are excellent representations of the aircraft. Each estimate is nearly indistinguishable from the truth values throughout the maneuvering.

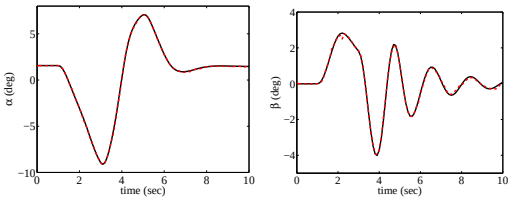

Fig. 7. Aerodynamic Angles (solid) and Estimates (dashed)

Finally, the estimates angles from Fig. 7 are used to improve the estimates of the translational velocities. The solutions to (17a)-(17c) are generated using the assumption of (18). The resulting velocity estimates, as shown in Fig. 8, are vastly improved from those in Fig. 5. Only minor errors remain in the vertical and side components while the forward component remains somewhat erroneous due to its sensitivity to the assumption of (18).

V. CONCLUSION

This paper has presented a technique for partial aircraft state estimation using vision as a sensor. Optical flow is used to compute accurate estimates of the aircraft body axis angular rates as well as the aerodynamic angles that determine the orientation of the velocity vector. Development of this purely visual technique is a step towards using vision for flight control in complex and cluttered environments.

VI. ACKNOWLEDGMENTS

This work was supported jointly by the Air Force Research Laboratory and the Air Force Office of Scientific Research under F49620-03-1-0381 with Johnny Evers, Sharon Heise, and Todd Combs as project monitors.

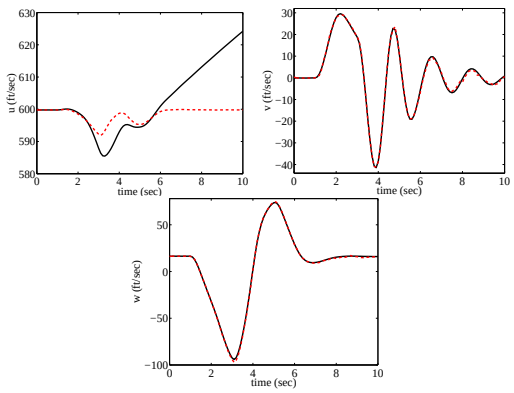

Fig. 8. Body Axis Velocities (solid) and Estimates (dashed) using Decoupled Optical Flow

REFERENCES

[1] Lucas, B., and Kanade, T., "An Iterative Image Registration Technique with an Application to Stereo Vision," *Proc. of the DARPA Image Understanding Workshop*, 1981, pp.121-130.

[2] Kanade, T., Amidi, O., and Ke, Q., "Real-Time and 3D Vision for Autonomous Small and Micro Air Vehicles," *43rd IEEE Conference on Decision and Control*, Paradise Island, Bahamas, December 2004.

[3] Yao, Y.S., Chellapa, R., "Dynamic Feature Point Tracking in an Image Sequence," 12^{th} *IAPR International Conference on Pattern Recognition*, Vol. 1, October 1994, pp. 654-657.

[4] Horn, B., and Schunck, B., "Determining Optical Flow," *Artificial Intelligence*, Vol. 17, pp. 185-203, October 1981.

[5] Beauchemin, S., and Barron, J., "The Computation of Optical Flow," *ACM Computing Surveys*, Vol. 27, No. 3, September 1995, pp. 433-467.

[6] Soatto, S., Frezza, R., and Perona, P., "Motion Estimation via Dynamic Vision," *IEEE Transactions on Automatic Control*, Vol. 41, No. 3, 1996, pp. 393-413.

[7] Soatto, S., Perona, P., "Recursive 3-D Visual Motion Estimation Using Subspace Constraints," *International Journal of Computer Vision*, Vol. 22, No. 3, 1997, pp. 235-259.

[8] Gurfil, P., and Rotstein, H., "Partial Aircraft State Estimation from Visual Motion Using the Subspace Constraints Approach," *Journal of Guidance, Control, and Dynamics*, Vol. 24, No. 5, 2001, pp. 1016-1028.

[9] Webb, T., Prazenica, R., Kurdila, A., and Lind, R., "Vision-Based State Estimation for Autonomous Micro Air Vehicles," *Proc. of the AIAA Guidance, Navigation, and Control Conference*, AIAA-2004-5349, Providence, RI, August 2004.

[10] Webb, T., Prazenica, R., Kurdila, A., and Lind, R., "Vision-Based State Estimation for Uninhabited Aerial Vehicles," *Proc. of the AIAA Guidance, Navigation, and Control Conference*, AIAA-2005-5869, San Francisco, CA, August 2005.

[11] Gebert, G., Snyder, D., Lopez, J., Siddiqi, N., and Evers, J., "Optical Flow Angular Rate Determination," *Proc. of the International Conference on Image Processing*, Vol. 1, 2003, pp. 949-52.

[12] Causey, R., and Lind, R., "Aircraft-Camera Equations of Motion," *AIAA Journal of Aircraft*, In Preparation.

[13] Ma, Y., Soatto, S., Kosecka, J., Sastry, S.S., *An Invitation to 3-D Vision: From Images to Geometric Vision*, New York, NY:Springer-Verlag, 2004.

[14] Roderick, A., Kehoe, J., and Lind, R., "Vision-Based Navigation Using Multi-Rate Feedback from Optic Flow and Scene Reconstruction," *Proc. of the AIAA Guidance, Navigation, and Control Conference*, AIAA-2005-6093, San Francisco, CA, August 2005.

[15] Branca, A., Stella, E., and Distante, A., "Passive Navigation using Focus of Expansion," *Proc. of the* 3^{rd} *IEEE Workshop on Applications of Computer Vision*, Sarasota, FL, December 1996, pp. 64-69.

[16] Nguyen, L, Ogburn, M., Gilbert, W., Kibler, K., Brown, P., and Deal, P., "Simulator Study of Stall/Post-Stall Characteristics of a Fighter Airplane with Relaxed Longitudinal Static Stability," Tech. Report 1538, NASA Langley Research Center, Hampton, VA, 1979.